

## Chapter 8

### INTRODUCTION

It is evident that the generalized micro-scale details of continuous fiber composite materials exert a profound influence on a laminate's performance. For instance, simply altering the matrix toughness can significantly affect damage initiation and development during static and fatigue loading<sup>8.1,8.2</sup>. The microstructure of the tough matrix maximizes the work of fracture, and dissipates the local energy so as to prevent premature failure. Enhancing fiber properties by extreme orientation and alteration of the graphitic crystallite size leads to increased tensile strength and stiffness. However, these gains in tensile performance are offset by significant reductions in compression strength and, once again, careful attention to the microstructure is required in order to control properties.

Recently, interest has grown in trying to understand a region/constituent that can have exceptional influence on composite performance, despite making up less than 1% of the composite. This small but important region is called the *interphase*<sup>8.3,8.4</sup>. Here the *interface* is defined as a distinct two-dimensional boundary, which defines for instance, where a fiber ends, and the binder begins. Most, but not all, investigators of composite performance believe that an *interphase* region and not just an *interface* is developed and exists in fiber composites. One needs only to look to a few of the most noted journals on composites to find extensive discussion of the *interface* and *interphase*. Although the above mentioned points will improve our understanding of the interphase, there is already considerable experimental evidence in the literature<sup>8.5-8.12</sup> to support the idea that proper arrangement of material and micro-structure within an interphase zone will, through a unique synergism, result in enhanced composite properties. In order to model this interfacial region's influence on composite performance, micro-mechanical models need to be employed. Reifsnider<sup>8.13</sup> made use of this concept by using micromechanical models for both tension and compression strength of laminates made with a poly(vinylpyrrolidone), PVP and Epoxy sizings to predict their fatigue response. This was achieved by understanding that during the process of fatigue, damage develops in the composite and things like cracks etc. change the local stresses. In addition, material strengths also tend to change due to degradation processes like chemical and physical

aging etc. The micro-mechanical representations of strength can however be used to track these changes and make complex predictions such as fatigue life possible through remaining strength arguments.

## **EXPERIMENTAL**

### **Materials**

The K-90 PVP sizing material (LUVISKOL lot # 20421501) (Figure 1 (a)) was obtained from BASF<sup>8,14</sup>. The  $M_w$  of this material was 1,250,000 g/mol and it had a  $T_g$  of 180°C. This material was dried at 110°C for 18 hours before being used.

The modified polyhydroxyether (Phenoxy<sup>TM</sup>) sizing material (PKHW-35 lot # 217013) (Figure 1 (b)) was obtained from Phenoxy Associates, Rock Hill, SC. This material was obtained as a 35 weight percent dispersion of approximately 1-micron diameter particles in water. The  $M_n$  of the Phenoxy was 19,000 g/mol (GPC) and it had a  $T_g$  of 97°C (DSC). Isopropanol used to break the Phenoxy<sup>TM</sup> emulsion was HPLC grade (lot # B5417) obtained from Burdick and Jackson. A detailed explanation of the sizing of Hexcel AS-4 carbon fibers with the above mentioned thermoplastics and the pultrusion process can be found in reference (8.15).

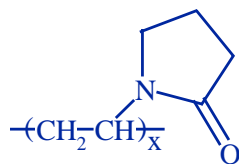
Dow 441-400 vinyl-ester resin (Figure 1 (c)) was obtained from the Dow Chemical Company. The resin consisted of 70wt% vinyl-ester oligomer and 30wt% styrene monomer (Figure 1 (d)).

The sizing/Derakane<sup>TM</sup> blends were cured with benzoyl peroxide (BPO). The BPO utilized for this purpose was obtained from Aldrich. The material was 97% pure (lot # ES 03918CS).

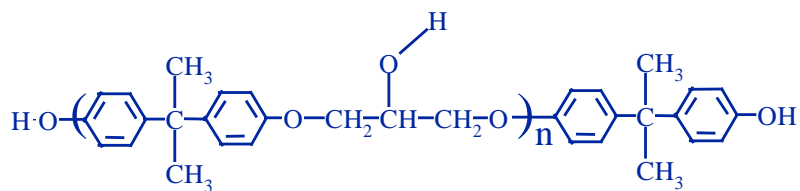
### **Fabrication of laminates for Shear Testing**

In order to assess the shear response of the different sizings,  $[\pm 45]_6$  laminates were prepared using the resin infusion process. A custom mold was designed for the RFI process<sup>8,16</sup>. The bottom of the mold was covered with a porous, teflon coated, fiberglass release cloth. Approximately 100g of the initiator charged Derakane 441-400 resin was poured into the mold cavity. The fibers were sized using the sizing process described in (8.17). The individual plies were placed one by one on top of the resin keeping in mind

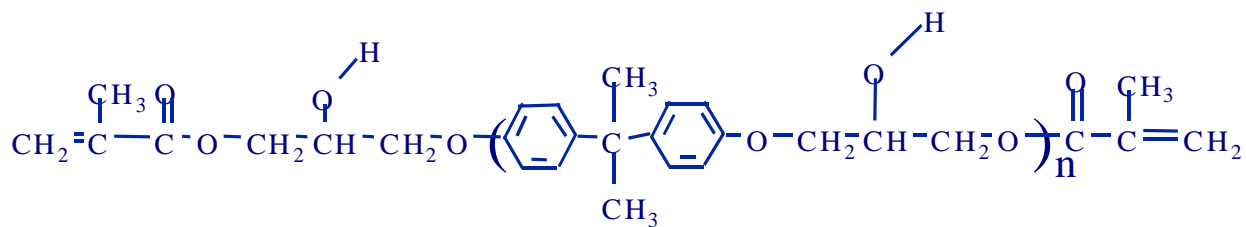
a).



b).



c).



d).

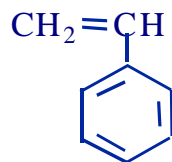


**Figure 1** a). Chemical structure of poly(vinylpyrrolidone) (PVP) sizing material. b). Chemical structure of poly(hydroxyether) sizing material. c). Chemical structure of vinyl-ester and d). Chemical structure of styrene monomer.

the desired orientation. The top surface of the fibers was covered with another piece of the porous teflon release cloth. A hole was placed in the center of the release cloth to allow resin to exit the cavity.

The piston plate (top of the mold) was placed on top of the fibers in such a way as to minimize pressure exerted on the fibers. The piston plate was designed with three distinct features. First, an o-ring around the piston plate was used to minimize resin leakage from the sides of the mold. Secondly, a 3 mm diameter hole in the center of the piston plate allowed excess resin to exit through the top of the mold. Finally, a trough was designed around the edges of the piston plate to allow excess resin to collect.

After the mold was assembled, it was placed in a Wabash (model 9112) 25 MPa vacuum hot press that had been covered with a 2 mm aluminum cover plate. The cover plate prevented excess resin from coming into contact with the press. The platens of the hot press were allowed to close at a rate of 6mm/min. The slow platen closure rate allowed the resin to fully impregnate the individual fabric plies while allowing the air and excess resin to exit. The platen closure pressure was 4000 KPa. The platens were then heated to 150°C at a rate of 15°C/min. The platens were held at 150°C for approximately 10 minutes then cooled to room temperature at a rate of -20°C/min. The platens were then opened and the composite panel was removed from the mold. All the composite panels were produced under the same processing conditions to insure that the same time was available for sizing diffusion.

### **Preparing blends for tensile testing**

A set of K-90 PVP/Derakane™ 441-400 vinyl-ester blends were prepared at compositions of 0.25, 1.00, 3.00, and 5.00 wt% K-90 PVP. The Derakane™ was added to a one-quart mason jar. An Arrow 850 high torque stirrer was placed into the Derakane™ and stirring was set at the maximum speed. The K-90 PVP was slowly added to the Derakane™ at a point where the vorticity appeared to be the greatest. If the K-90 PVP was added to quickly, then the PVP would clump and not dissolve. However, if the K-90 PVP was added to slowly, then the PVP would start to significantly dissolve before all the PVP had been added. This greatly increased the solution viscosity and made the adding of additional PVP impossible. After all the K-90 PVP had been added to the Derakane™, the mixture was allowed to rapidly stir until all of the K-90 PVP had been

dissolved (approximately 24 hours for the 5.0 wt%). Some of the resulting K-90/Derakane™ blends were utilized for dielectric analysis and density determination (note: after the blend had been catalyzed then the density was determined). Some of the blends were also used for the preparation of cured K-90 PVP/Derakane blends.

### **Density determination of the un-cured blends**

The density of the un-cured K-90 PVP/Derakane™ blends was determined utilizing a Fisher Scientific grease pycnometer. The assembled pycnometer was weighed empty and then full of deionized water at ambient temperature. The pycnometer was carefully dried. The K-90 PVP/Derakane™ blend was added to the pycnometer base while insuring that no air bubbles were trapped. The pycnometer was reassembled and weighed. The density of the blend was determined from the following equation.

$$\rho_u = \frac{(m_u - m_{pyc})}{(m_{water} - m_{pyc})} \quad (1)$$

where  $\rho_u$  was the density of the un-cured blend,  $m_{blend}$  was the mass of the pycnometer filled with the blend,  $m_{pyc}$  was the mass of the pycnometer,  $m_{water}$  was the mass of the pycnometer filled with the water (note: all at the ambient temperature).

### **Curing of the blends**

The K-90 PVP/Derakane™ and the Phenoxy™/Derakane™ were cured utilizing benzoyl peroxide. A BPO concentration of 1.1 wt% in Derakane™ was utilized (or a 0.011:1 weight ratio of BPO to Derakane™). In order to keep the material systems somewhat similar, the same ratio of BPO to Derakane™ was utilized in these experiments. However, because the amount of sizing material varied from blend to blend, so did the actual concentration of BPO. The blend was added to a suitable glass container. An Arrow 850 high torque stirrer was placed into the blend and stirring was set at the medium speed. The BPO was slowly added to the stirring mixture. After the BPO had dissolved (approximately 1 hour), the blend was degassed utilizing approximately 24 in Hg vacuum. The blend was allowed to degas for approximately 30 minutes. The catalyzed K-90 PVP/Derakane™ blends were cured utilizing the following procedure. An 20.34 cm X 15.24 cm X 0.635 cm vertical mold was utilized for the curing process to prevent the formation of air voids. The mold was treated with mold

release and then assembled. The blend was added very slowly to the mold. Because the viscosity of some of the blends was so high, it was difficult preventing air from being trapped in the mold. In addition, the high viscosity prevented some of the blends from flowing into the corners of the mold. This was counteracted by heating the mold to a temperature above room temperature but below the initiation temperature of the Derakane™ and holding it there for a period of time. After the top had been secured to the mold, it was then placed in a Fisher Isotemp forced convection oven. The material was cured utilizing the following cure cycle: 1 hour hold at 65°C → heating at 10°C/min to 150°C → 20 minute hold at 150°C. After the mold had cooled to room temperature, the cured blend was removed.

### **Density determination of the cured blends**

The density of the cured blends was determined by applying Archimedes' principle. Approximately 6 grams of the cured blend was weighed. The sample was then immersed in isopropyl alcohol and weighed again. The density of the cured blend was calculated using Archimedes' principle using the following equation.

$$\rho_c = \rho_{IPA} \left[ \frac{W_{air}}{(W_{air} - W_{IPA})} \right] \quad (2)$$

where  $\rho_c$  = density of the cured blend,  $\rho_{IPA}$  = density of Isopropyl alcohol,  $W_{air}$  = weight of blend in air and  $W_{IPA}$  = weight of sample in isopropyl alcohol (note: all at ambient temperature).

### **Shrinkage of blends upon cure**

As the free-radical polymerization of the vinyl-ester network progresses, the density of the system correspondingly increases due to a decrease in system volume. The degree of volumetric shrinkage can be determined from the cured and un-cured blend densities utilizing the following equation.

$$\beta = 100 \left[ 1 - \left( \frac{\rho_u}{\rho_c} \right) \right] \quad (3)$$

where  $\beta$  is the percent blend shrinkage,  $\rho_u$  is the un-cured blend density computed from equation (1), and  $\rho_c$  is the cured blend density computed from equation (2).

### Misalignment angle assessment

The misalignment angle is crucial to any compression strength model. In order to measure the misalignment angle in the composite, a method discussed by Yurgartis<sup>8,18</sup> was used. Composite specimens were very carefully cut at an angle of 5° with respect to the direction of the fibers (figure 2) using a diamond blade on a Buehler Micromet<sup>®</sup>. The samples were then potted using a two part Buehler Epoxide<sup>™</sup> resin and left to cure at room temperature for 8 hours. Next, the samples were ground on a Buehler grinding machine that comprised of an Automet 2<sup>®</sup> head and the Ecomet 3<sup>®</sup> table. Photographs of the polished surface were taken with the help of a Nikon, Epiphot<sup>®</sup> inverted optical microscope at a magnification of approximately 418X. Figure 3 shows a micrograph of the G' sized, unidirectional fiber reinforced composite. It can be seen that a distribution in lengths exists. In addition to which, there is additional distortion in the fibers as indicated in the figure. This distortion is not only due to a misalignment in a plane perpendicular to the paper but along the paper. This second mode of misalignment was not seen to exist with the Phenoxy or PVP K90 sized composites. The lengths of the roughly 20 individual fibers were measured using a Mitutoyo digital caliper. The unadjusted angles, 'ω', were calculated by

$$\sin(\omega) = \frac{d}{l} \quad (4)$$

where, d is the fiber diameter and l is the length of the major diameter as measured from the photograph. Since the sample was initially cut at an angle of 5° the final adjusted misalignment angle is,

$$\phi = \omega - \phi_i \quad (5)$$

where φ is the misalignment angle, ω is the calculated unadjusted angle and φ<sub>i</sub> is the angle at which the sample was cut namely 5° in this case.

The distribution in angles for the individual composites is presented in figures 4, 5 and 6. The mean angles from the normal distribution are, 1.75° for the PVP K90, 1.15° for the Phenoxy and 3.03° for the G' sized composites (table 1).

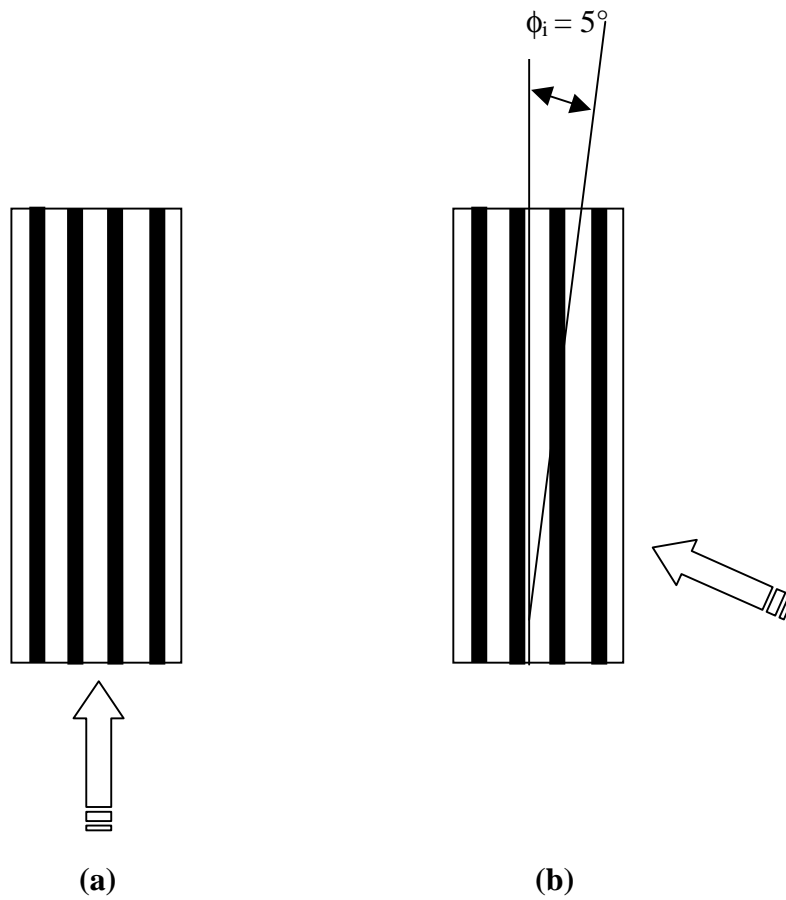


**Figure 2:** Schematic of unidirectional composite specimens used for (a) fiber diameter and (b) misalignment calculations. The arrow indicates the direction the sample was viewed on the microscope.

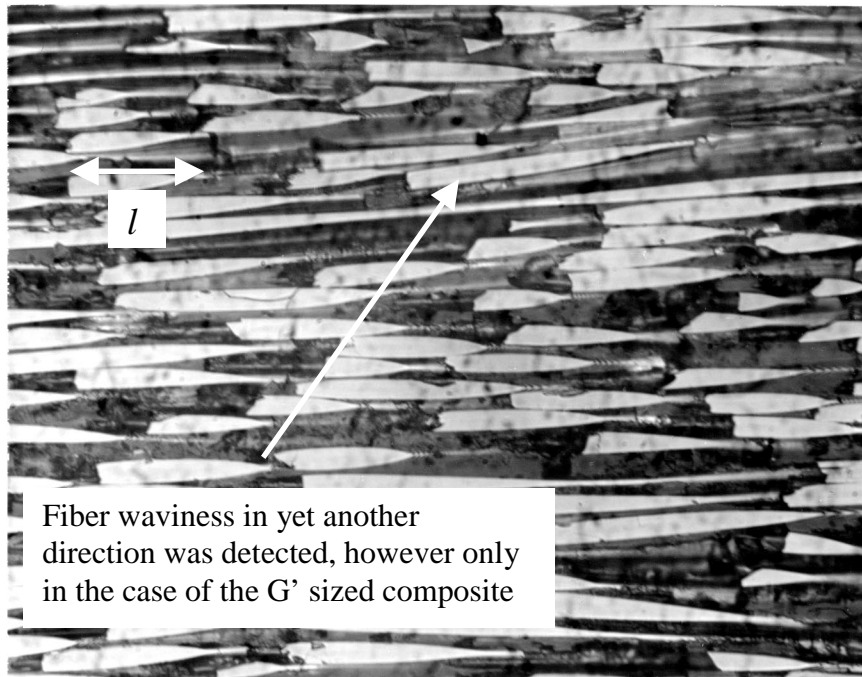


**Figure 3:** Optical micrograph of a section of the G' sized composite that was cut at an angle of  $5^\circ$  to the direction of the fibers. Micrographs similar to this were used to measure initial fiber misalignment angle for the individual composites. The magnification as measured using a stage micrometer with a least count of 0.01 mm is  $1 \text{ mm} = 2.4 \mu\text{m}$

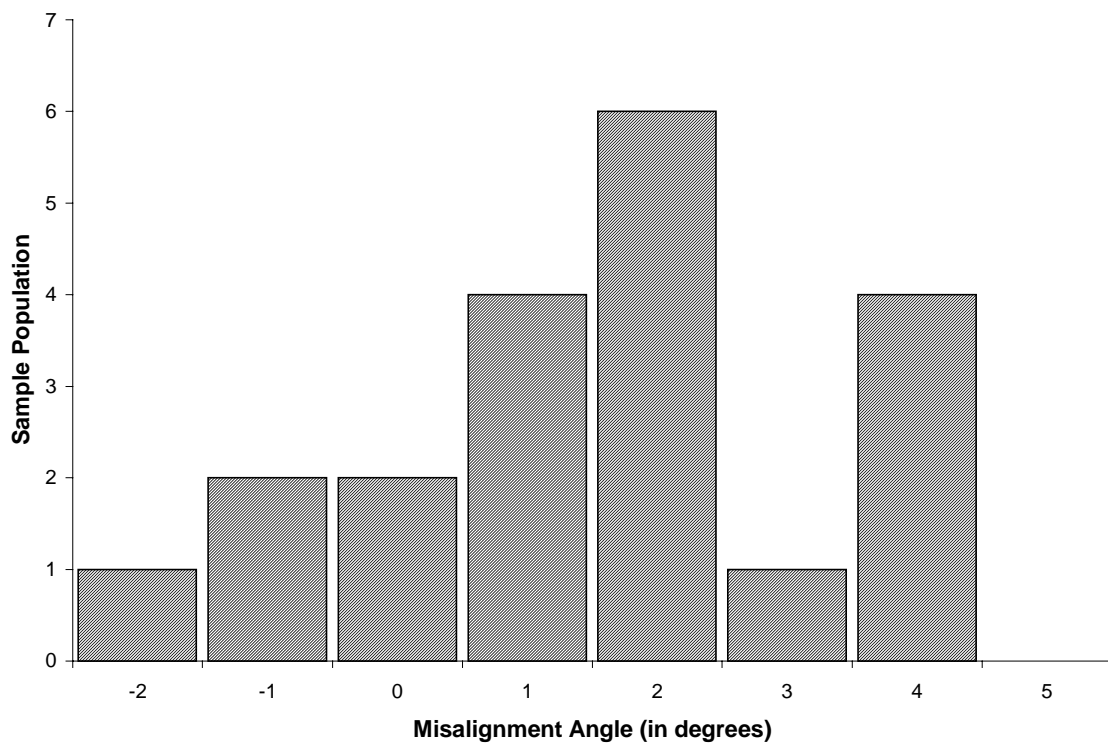


**Figure 4:** Misalignment angle distribution for unidirectional PVP K90 composites. The normal distribution mean is  $1.75^{\circ}$  with a standard deviation of 1.6

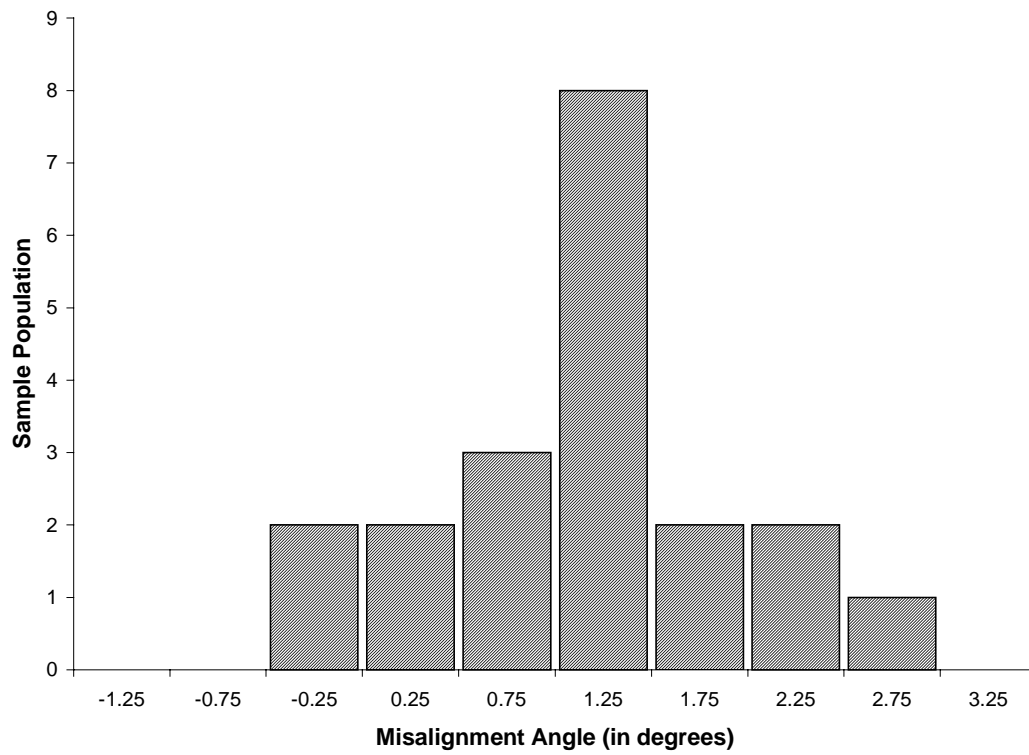


**Figure 5:** Misalignment angle distribution for unidirectional Low spread Phenoxy composite. The normal distribution mean is  $1.15^\circ$  with a standard deviation of 0.75

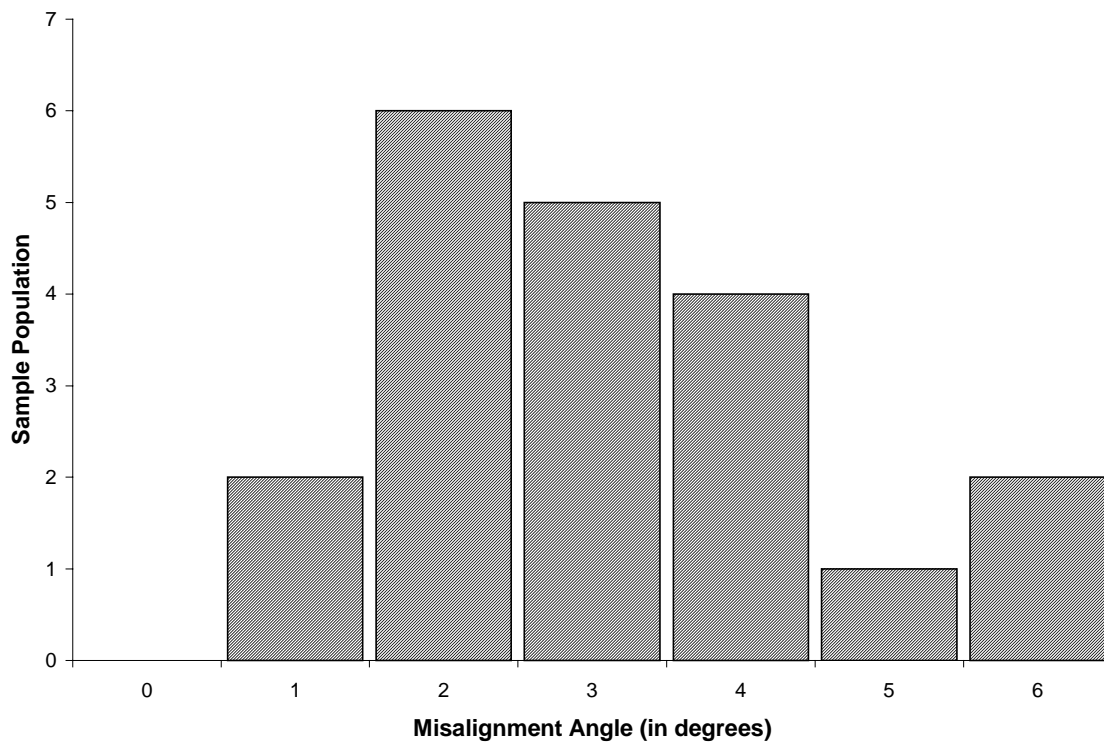


**Figure 6:** Misalignment angle distribution for unidirectional G' composite. The normal distribution mean is  $3.03^\circ$  with a standard deviation of 1.4

**Table 1:** Properties used in the models for the different composite systems

| Composite Type | Fiber Diameter (in $\mu\text{m}$ ) <sup>1</sup> | Fiber Tensile Modulus (in GPa) <sup>2</sup> | Fiber Strain to Failure (in %) <sup>2</sup> | Fiber Volume Fraction <sup>3</sup> | Average Misalignment Angle (in degrees) <sup>1</sup> |
|----------------|---|---|---|------------------------------------|--|
| G' Sizing      | 6   | 262   | 1.56  | 0.656                              | 3.03   |
| PVP K90 Sizing | 7.2   | 252   | 1.63  | 0.61                               | 1.75   |
| Phenoxy Sizing | 7.2   | 252   | 1.63  | 0.61                               | 1.15   |

<sup>1</sup> Measured experimentally using sectional scanning electron micrographs of the cross-section.

<sup>2</sup> Obtained from Hexcel Corporation

<sup>3</sup> Theoretically computed

In addition, since the exact imperfection wavelength is difficult to obtain, the present data is presented in the form of a parametric study for different L/a ratios.

### **Mechanical testing**

The  $[\pm 45]_6$  laminates were cut into strips, 15.24 cm X 2.54 cm using a water cooled table saw. The edges were ground to ensure that the edges were parallel. In order to measure strain accurately, two foil strain gages supplied by Micromeritics™ were used along with a 2.54 cm gage length MTS™ extensometer. The two 350 $\Omega$  gages were bonded using a cyanoacrylate ester, M-Bond, adhesive package supplied by Micromeritics. The surface of the specimens was lightly sanded using 600-grit sandpaper. The gages were then bonded at right angles to each other at the center of the specimen. Lead wires were then soldered onto the gages in preparation for testing. On the reverse side, two aluminum tabs notched for mounting the extensometer were bonded to the specimen using a GE, RTV silicone grease. The specimen was cured in an oven at 50°C for 1 hour to ensure cure of the RTV adhesive. Quasi-static tensile tests were performed on the specimens using a screw driven Instron load frame. A loading rate of 2

mm/min was used for the tests. Signals from the foil gages were fed into a Vishay™ 2310 amplifier and processed by Labview™ along with the crosshead displacement, load and extensometer signals.

The polymer blend samples were first cut down into rectangular strips 18.78cm x 3.0cm using a water-cooled Buehler™ wafering blade. The samples were then ground in the machine shop in to ensure that the edges were square and dimensions were accurate. The machined strips were then machined into the ASTM D690 stipulated dog-bone shape by hand feeding them into a table router. The final tensile samples were 17.78cm x 2.54cm. The edges were then hand-sanded wet using 600-grit sandpaper. Aluminum extensometer tabs were adhesively bonded to the specimen as explained in the previous paragraph and tensile tests were performed on a screw driven Instron load frame. A loading rate of 2mm/min was adopted in accordance with the standard. Again, data concerning the load, strain and crosshead displacement were monitored using Labview™.

## **RESULTS AND DISCUSSION**

This paper shares results on the density measurements of the uncured and cured blends and the resulting shrinkage. It also focuses on the use of micro-mechanical models to estimate both the tensile and compressive strength of the sized composites. Details regarding the glass transition of the blends as measured by differential scanning calorimetry are outlined in detail in reference (8.19).

### **Density determination of the un-cured blends**

The density of the un-cured K-90 PVP/Derakane™ were determined as a function of K-90 PVP concentration in the Derakane™ (Figure 7 (a)). The density followed a linear behavior versus concentration. If the K-90 PVP/Derakane™ system were to have behaved ideally over the entire concentration range, then the theoretical pure K-90 PVP density should have been approximately 2.67 g/ml. The pure K-90 PVP density was approximately 1.20 g/ml which was an indication of a positive deviation from ideal mixing. Li and co-workers<sup>8,20</sup> showed similar trends with K-90 PVP and Derakane™. They attributed this non-ideality to the large extent of hydrogen present between the K-90 PVP and the vinyl-ester portion of the Derakane™.

### **Density determination of the cured blends**

The density of the cured K-90 PVP/Derakane™ were determined as a function of K-90 PVP concentration in the Derakane™ (Figure 7 (b)). The cured blend density was found to be constant and not a function of K-90 PVP in Derakane™ concentration. This result was surprising considering the fact that the un-cured blend density showed a strong dependence on K-90 PVP concentration. Assuming the same degree of matrix cure, this would imply a decrease in matrix shrinkage as a function of increasing K-90 PVP in Derakane™ composition as will be discussed in the next section.

### **Shrinkage of Blends upon Cure**

The shrinkage of the blends upon cure was computed from equation 3 (Figure 8). The results showed that the shrinkage decreased with increasing K-90 PVP in Derakane™ concentration. The shrinkage showed a 4-fold decrease from the pure Derakane™ value of 8.3% to 1.9% for the 5.0wt% K-90 PVP. This has positive implications for the interphase region where shrinkage induced fiber/matrix interface cracking is known to be a problem with the Derakane™ system. If an interphase were to have formed from the K-90 PVP sizing, then a reduction in shrinkage induced fiber/matrix interface cracking would be expected.

### **Tensile Strength Model**

To capture the effects of the interface of tensile strength, a model developed by Subramanian, Reifsnider and Stinchcomb<sup>8,21</sup>. Details regarding the equations of the model can be found in the reference. An ‘efficiency’ parameter of the interface is introduced to account for the effectiveness of load transfer from the matrix to the fibers. The interface is also characterized by the interfacial shear strength. These two parameters are needed to capture the effect of stress concentration in fibers adjacent to the broken fibers and the ineffective length.

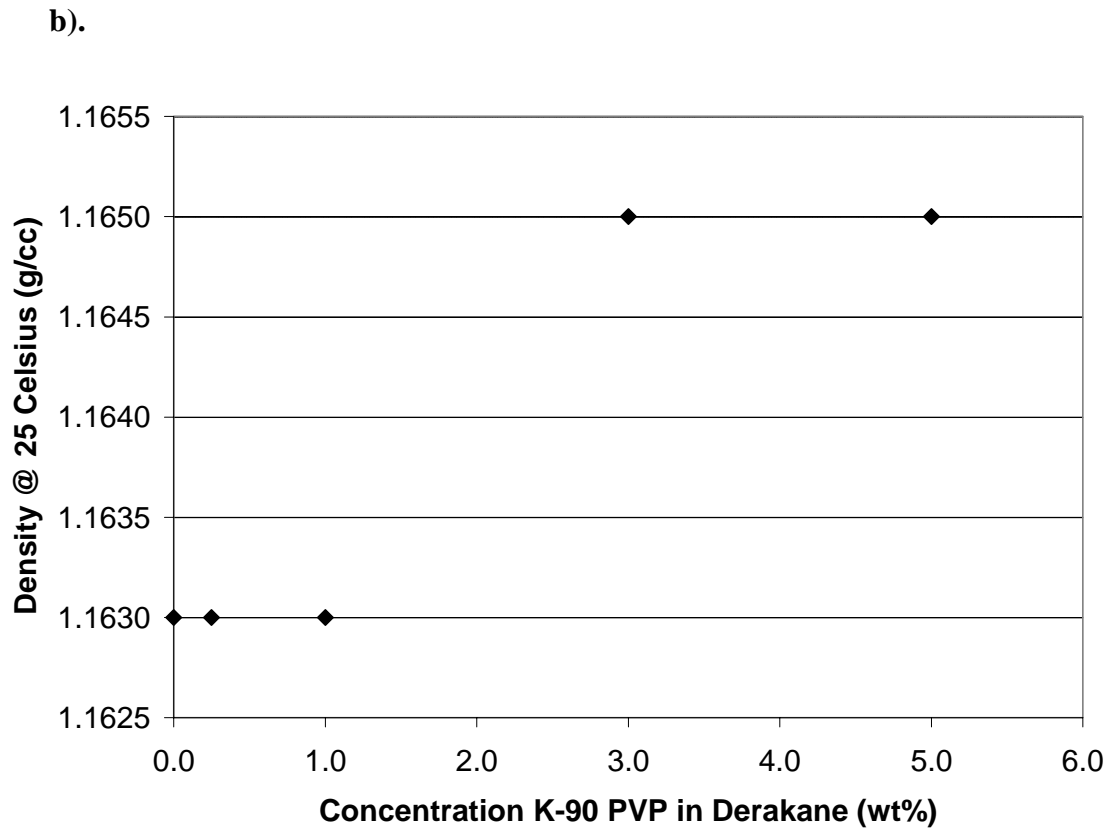
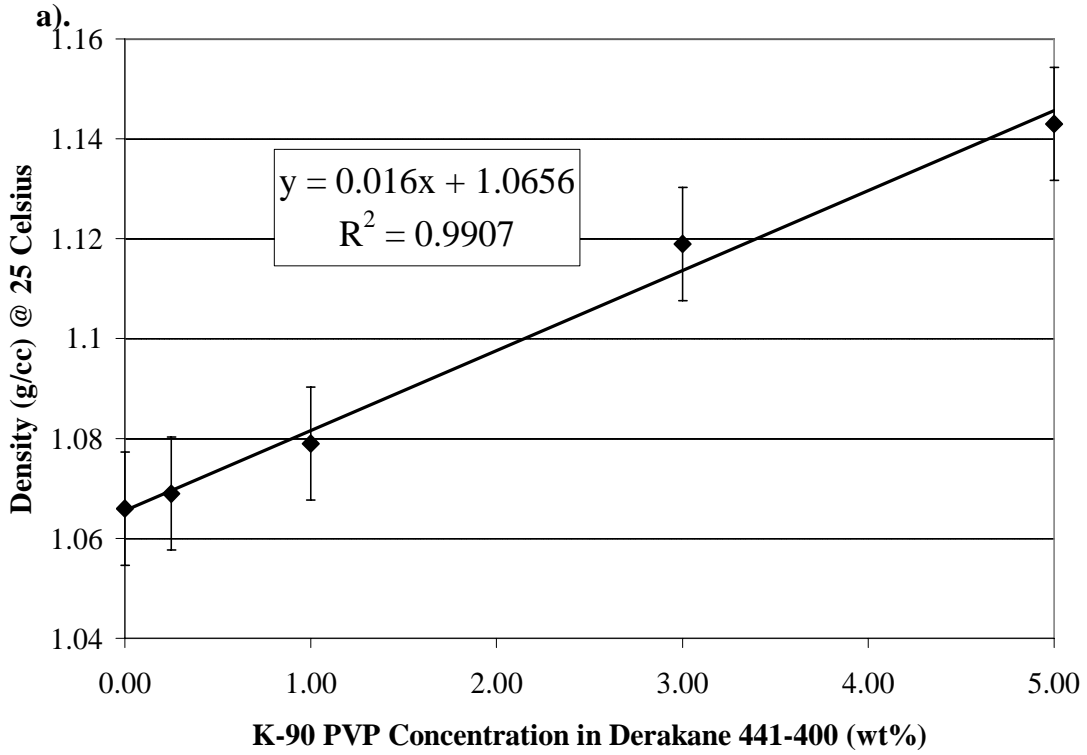


**Figure 7:** Density at 25°C for K-90 PVP in Derakane™ blends. a). un-cured b). cured.

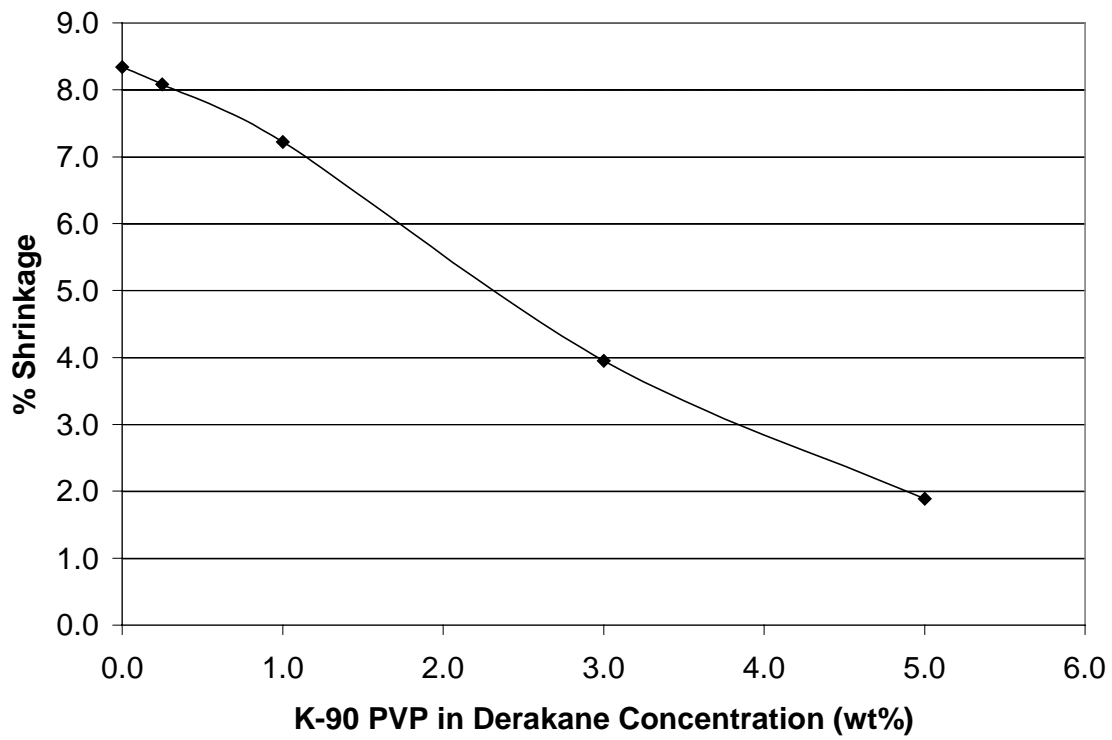


**Figure 8:** Percentage blend shrinkage as a function of K-90 PVP in Derakane™.

The interphase in this model is reduced to a two dimensional region. In this model the broken fibers are assumed to form a central core with a layer of matrix material around it. A concentric cylinder of neighboring fibers is assumed to surround this central core. This type of formulation is based on some previous work done by Gao and Reifsnider<sup>8,22</sup>. In constructing the force equilibrium equations for the core of broken fibers and adjacent fibers, it is assumed that the entire axial load is taken up by the fibers and that the load is transferred between fibers via shear. Hence the matrix material between adjacent fibers to the broken core is neglected. It is also assumed that the displacements in the fiber and matrix at the fiber-matrix interface are discontinuous, and that the average displacement in the composite is uniform. This then yields the following expressions for the displacements,

$$u_c = \frac{\sigma_a x}{E_x} \quad (6)$$

$$u_{f1} = \eta u_{m1} \quad (7)$$

$$u_{f2} = \eta u_{m2} \quad (8)$$

where  $u_{f1}$  and  $u_{f2}$  are the fiber displacements at the different locations shown in Figure 9. Substituting these along with the linear shear response equations, the equilibrium equations take the following form

$$\frac{d^2 u_{f1}}{dx^2} + k_1 u_{f1} + k_2 u_{f2} = 0 \quad (9)$$

$$\frac{d^2 u_{f2}}{dx^2} - k_3 u_{f2} + k_4 u_{f1} + k_5 x = 0 \quad (10)$$

where,

$$\begin{aligned}
k_1 &= -\frac{2r_{f1}G_m}{bE_{f1}\eta r_{f2}^2} \\
k_3 &= \frac{2r_m G_m}{n_i b E_{f2} \eta r_{f2}^2} + \frac{2r_{f2} G_m}{n_i b E_{f2} \eta r_{f2}^2} \\
k_4 &= \frac{2r_m G_m}{n_i b E_{f2} \eta r_{f2}^2} \\
k_5 &= \frac{2r_{f2} G_m \sigma_a}{n_i b E_{f2} \eta r_{f2}^2 E_x}
\end{aligned} \tag{11}$$

The boundary conditions used are,

$$\begin{aligned}
\left( \frac{du_{f1}}{dx} \right)_{x=0} &= 0 \\
(u_{f2})_{x=0} &= 0
\end{aligned} \tag{12}$$

The differential equations are solved and the solution yields the displacements,  $u_{f1}$  and  $u_{f2}$ . Next, the strains and stresses in the central core and adjacent fibers are derived using the constitutive equations for stress-displacement. These are given as follows,

$$\begin{aligned}
\varepsilon_{f1} &= \frac{du_{f1}}{dx}; \quad \sigma_{f1} = E_{f1} \varepsilon_{f1} \\
\varepsilon_{f2} &= \frac{du_{f2}}{dx}; \quad \sigma_{f2} = E_{f2} \varepsilon_{f2}
\end{aligned} \tag{13}$$

Next, stress concentration factors and ineffective lengths are defined for both the elastic and plastic case. It is assumed that the matrix exhibits an elastic-perfectly plastic behavior. If the average stress in the matrix exceeds the interfacial shear strength, the interface is assumed to be debonded. Once this occurs, the shear stress in the matrix is

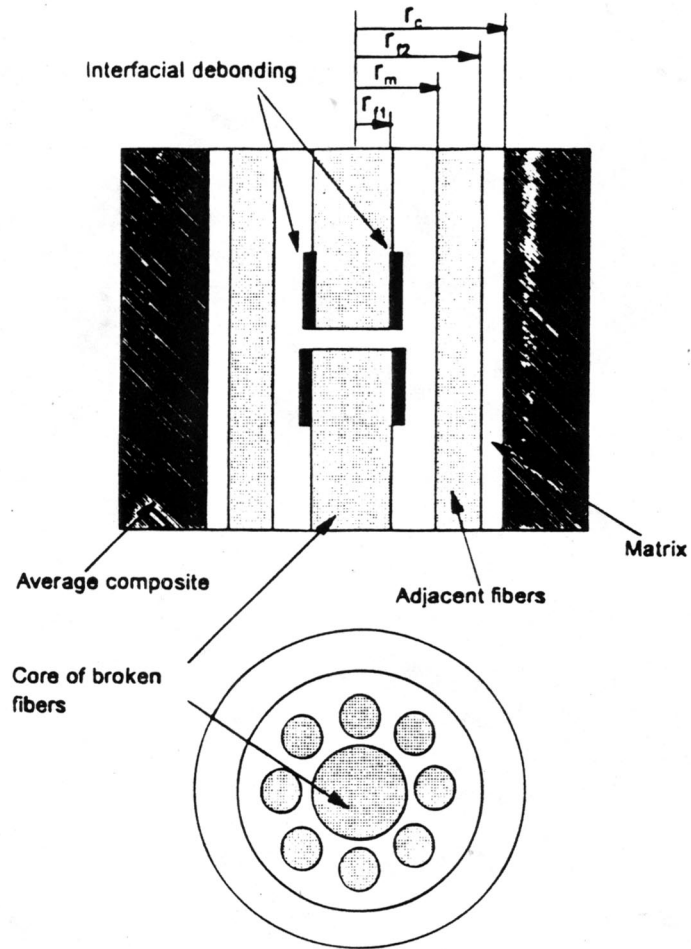


**Figure 9:** Schematic of the arrangement of the concentric cylinders of broken fibers, adjacent fibers and unaffected composite (reference 8.20)

assumed to be constant over the region defined as the plastic ineffective length and zero elsewhere. Once these factors are defined, the tensile strength is calculated using Batdorf's analysis<sup>8.23</sup>. At each load level, the average shear stress in the matrix is calculated and compared with the interfacial shear strength. If it has then debonding is assumed to have occurred and the plastic stress factor and ineffective lengths are used to predict fiber fractures and the failure is termed as plastic. If on the other hand no interfacial failure until instability occurs, then the failure is said to be elastic.

A computer code written by the authors of the model was used to calculate the tensile strength of the phenoxy composite. An interfacial shear strength of 44 MPa for the phenoxy was taken from a previous publication<sup>8.24</sup>. The predicted value of tensile strength for the phenoxy-sized composite was 2137 MPa as compared to the experimental values of  $1940 \pm 72$  MPa for the high spread case and  $2035 \pm 35$  MPa for the low spread case. The authors feel that this is a reasonable prediction and will further validate its use by testing it for the other sized composites. The interfacial strength values are however the limitation at present.

#### **$\pm 45^\circ$ Laminate Shear Data**

Figure 10 show the representative shear stress-strain curves for the three sizings. A couple of interesting observations can be readily made, namely, the response changes from being elastic and brittle for the G' sizing to elastic-perfectly plastic for the PVP K90 sizing. As a result of which, strain to failure changes tremendously. This is extremely interesting and important considering that only the sizing has changed in the composites. In the case of the G' composite, upon reaching a critical strain, surface cracks develop and complete failure occurs soon after that. For the PVP K90 however, crack saturation occurs and results in the system being pulled in a plastic manner to failure. The strain gages used were only calibrated to measure 5% strain as a result of which failure has not been denoted on the stress strain plot for the PVP K90 system. The extensometer attached to the back surface of the specimen measured strains as high as 12% at which point separation of the sample was observed. Figures 11 and 12 show the strength and modulus comparisons for the different composites. In addition to the change in loading response, the shear modulus and strength appear to be different. Changes in shear response of this nature are extremely important for the compression strength models.

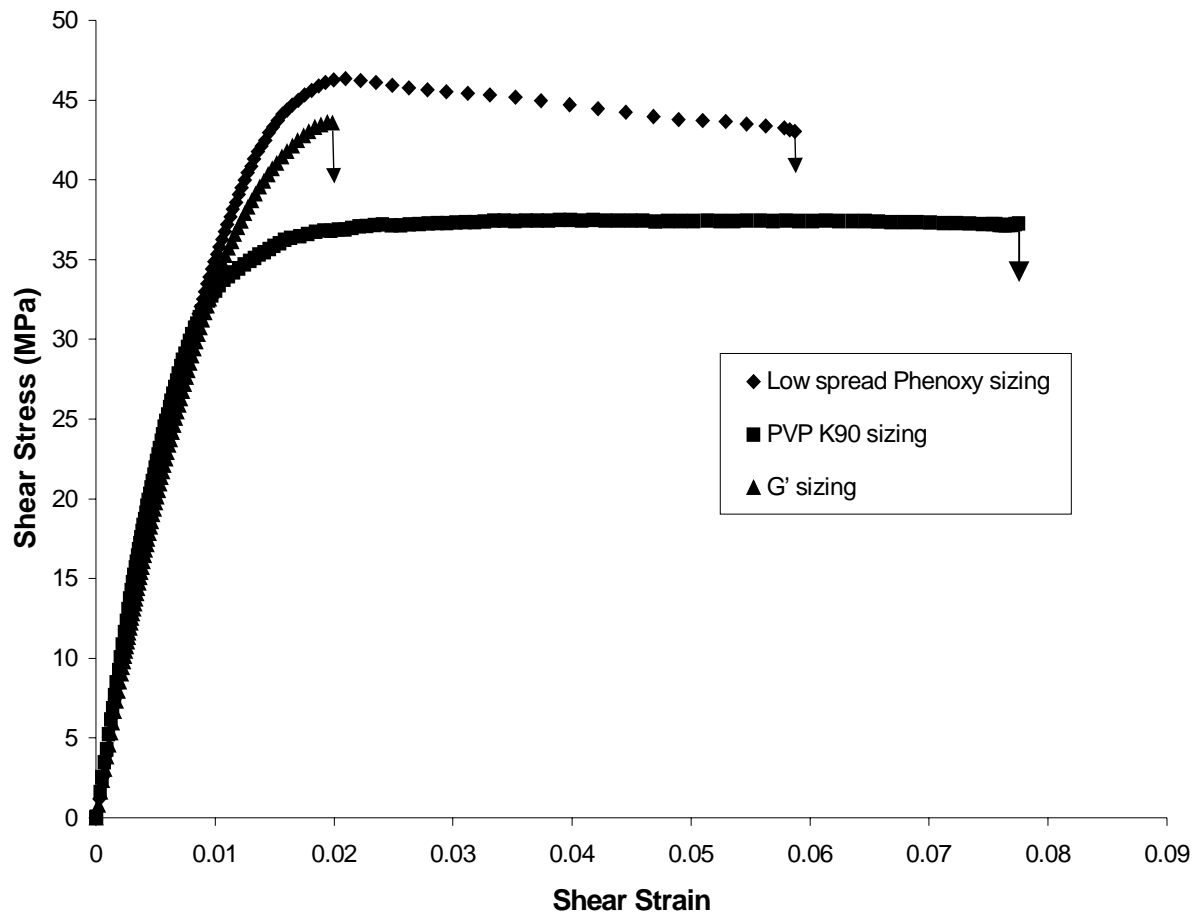


**Figure 10:** Comparison of shear stress versus strain response for composites with different fiber sizings. Data obtained from tensile tests performed on  $[\pm 45]_6$  laminates

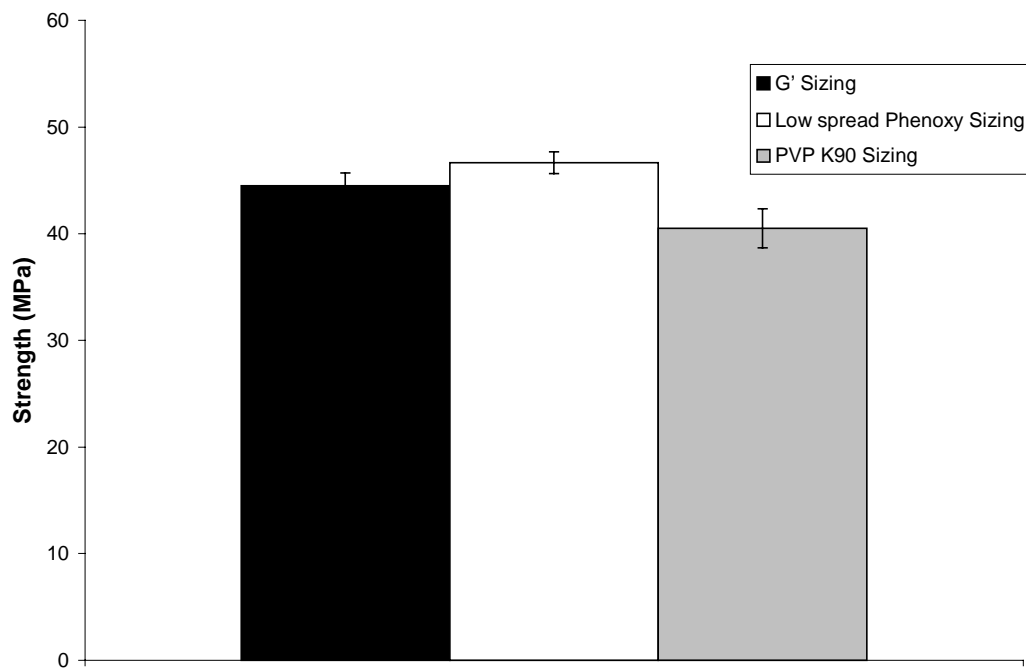


**Figure 11:** Comparison of shear strengths for composites with different fiber sizings. Data obtained from tensile tests performed on  $[\pm 45]_6$  laminates

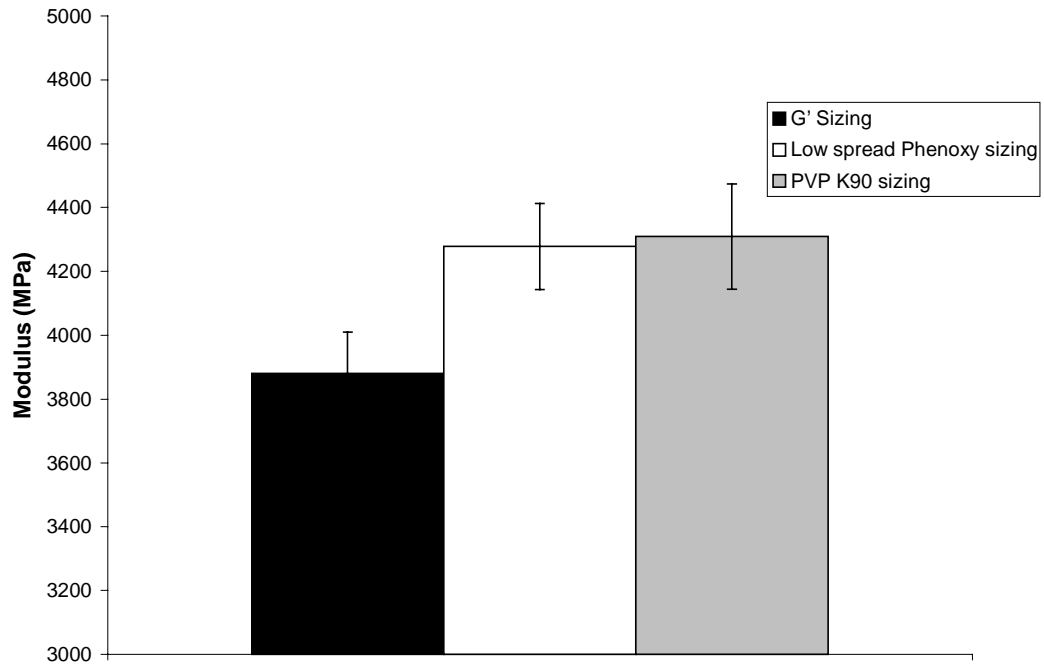


**Figure 12:** Comparison of shear modulus for composites with different fiber sizings. Data obtained from tensile tests performed on  $[\pm 45]_6$  laminates

## Compression Strength Models

In the evolution of models designed to predict compression strength, the work of Rosen<sup>8.25</sup> is pioneering. In a classic study based on slender columns on an elastic foundation, he suggested that the compression strength depends only on the initial matrix shear modulus and fiber volume fraction of the composite. Compression strength according to him was defined as follows,

$$\sigma_c = \frac{G_m}{1 - v_f} \cong G \quad (14)$$

where  $G_m$  is the matrix shear modulus,  $G$  is the composite shear modulus and  $v_f$  is the fiber volume fraction of the composite. The above expression assumes that the shear mode of deformation is the prevalent failure mode. The model however significantly over predicts the compression strength. Argon<sup>8.26</sup> suggested the use of an initial misalignment of the fibers to account for this. He took care of both the effects of plasticity and initial misalignment and an expression as follows was put forth,

$$\sigma_c = \frac{\tau_y}{\bar{\phi}} \quad (15)$$

where  $\tau_y$  and  $\bar{\phi}$  are the composite shear yield stress and initial misalignment angle respectively. Both the above models however neglected the fact that in practice, the kink band is inclined to the transverse direction thereby making the critical stresses somewhat higher.

### Model 1

Budiansky<sup>8.27</sup> encompassed both the results by assuming an elastic-perfectly plastic composite shear response. The equation is as follows,

$$\sigma_c = \frac{\tau_y}{(\gamma_y + \bar{\phi})} = \frac{G}{\left(1 + \frac{\bar{\phi}}{\gamma_y}\right)} \quad (16)$$

In the above equation, the shear response is defined as follows,

$$\begin{aligned} \tau &= G\gamma \quad \text{for } \gamma < \gamma_y \\ \tau &= \tau_y \quad \text{for } \gamma > \gamma_y \end{aligned} \quad (17)$$

where  $\gamma_y$  is the yield shear strain of the composite

### **Model 2**

Subsequently, Budiansky and Fleck<sup>8,28</sup> modified the above result to include material strain hardening. Assuming a Ramberg-Osgood shear stress-strain relation which is given by

$$\frac{\gamma}{\gamma_y} = \frac{\tau}{\tau_y} + \left(\frac{3}{7}\right) \left(\frac{\tau}{\tau_y}\right)^n \quad (18)$$

where  $n$  is the strain hardening index ( $3 < n < \infty$ ) and  $\tau$  and  $\gamma$  are the shear stress and strain respectively. Using the above, they obtained an expression for compression strength given by

$$\sigma_c = G \left[ 1 + n \left(\frac{3}{7}\right)^{\frac{1}{n}} \left(\frac{\bar{\phi}}{\gamma_y(n-1)}\right)^{\frac{n-1}{n}} \right]^{-1} \quad (19)$$

The present paper uses both equations 13 and 16 to predict compression strength and table 2 shows the results obtained against that measured experimentally.

### **Model 3**

The present paper also makes use of a model developed by Stief<sup>8,29</sup>. The model is based on the premise that in order to microbuckle, the fibers must bend sufficiently to cause fiber breakage. The model is also based on the fact that in all composites a certain amount of misalignment exists. These misaligned bundles are allowed to undergo finite deformation. The matrix is assumed to have an approximately elastic-perfectly plastic shear resistance. The criterion for fiber breakage is that the total tensile strain in the fiber should exceed its failure strain. The shear deformation mode is chosen. A free-body diagram of an element of the representative fiber in the shear mode plane is shown in figure 13 (a). Figure (b) shows a schematic of an infinite kink band in a unidirectional composite<sup>8,30</sup>. Fibers within the composite have an initial misalignment angle of  $\phi_i$ . Figure (c) a sketch of a typical load versus end shortening curve with key event locations indicated on the curve.

**Table 2:** Comparison of theoretical (Models 1 and 2) and experimental compression strengths for the different unidirectional composites

| Composite Type | Composite Shear Modulus <sup>1</sup> (in GPa) | Composite shear yield Strain <sup>2</sup> (%) | Strain Hardening Index <sup>3</sup> , n | X <sub>c</sub> (in MPa) [Model 1] | X <sub>c</sub> (in MPa) [Model 2] | X <sub>c</sub> (in MPa) [Exp.] |
|----------------|---|---|---|-----------------------------------|-----------------------------------|--------------------------------|
| G'             | 3.88  | 0.0109  | 5.5                                     | 667.2                             | 630.07                            | 747±110                        |
| PVP K90        | 4.31  | 0.0083  | 14                                      | 1010.3                            | 1109.25                           | 932±84                         |
| Phenoxy        | 4.28  | 0.0083  | 5                                       | 1251.03                           | 1235.24                           | 913±98                         |

<sup>1</sup> Obtained experimentally from tensile tests on [ $\pm 45$ ]<sub>6s</sub> laminates

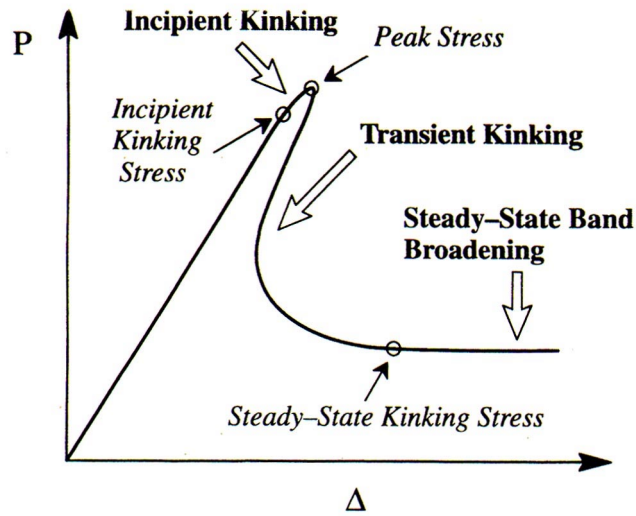
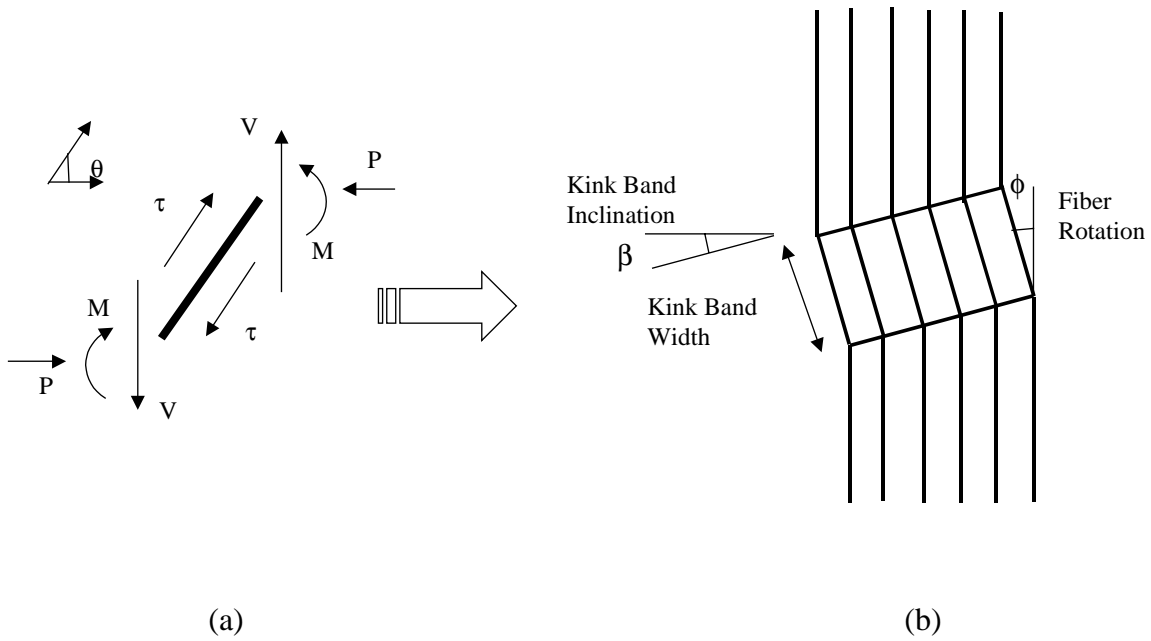
<sup>2</sup> Obtained using the 0.2% strain offset method

<sup>3</sup> Obtained from the Ramberg-Osgood fit to the experimental shear data

If the fiber is assumed to be circular with radius  $a$ , then the couple communicated to the fiber by shear stresses is equal to  $4a^2\tau$ . For a simple moment balance, the following equilibrium equation is established

$$\frac{dM}{ds} + P \sin \theta - 4a^2\tau = 0 \quad (20)$$

where  $P$  and  $M$  are the longitudinal compressive force and moment in the fiber. 's' is the arc length along the segment. The shearing force is assumed to be a pure couple thereby eliminating the transverse shear force everywhere and keeping the longitudinal force constant throughout the fiber.



(c)

**Figure 13:** (a) Free body diagram of the element of a micro-buckled fiber (reference 27), (b) Schematic of an infinite kink band in a uni-directional composites. Fibers within the composite have an initial misalignment angle of  $\phi_I$  and (c) a sketch of a typical load versus end shortening curve with the locations of key event indicated on the curve (reference 8.29).

Incorporating the constitutive laws at this point namely,

$$M = E_f I \frac{d\theta}{ds} \quad (21)$$

where  $E_f$  is the fiber modulus and  $I$  is the moment of inertia for the circular fiber. To obtain equation 14, it is assumed that the strains in the fiber are infinitesimal, even though the deflections are arbitrarily large. Treating the fiber as an elastica, the moment at each point is taken to be proportional to the local curvature.

The model is sensitive to fiber misalignment and the nature of the composite shear response in the model presented in Stief's paper this is taken to be elastic-perfectly plastic, which is given by the following equation,

$$\tau = \tau_c \tanh\left(\frac{G_L \theta}{\tau_c}\right) \quad (22)$$

The above equation is equal to  $G_L \theta$  for small  $\theta$  and is  $\tau_c$  for values of  $\theta$  that are large compared to  $\tau_c/G_L$ . The shear response of the composite could however be very easily changed to accommodate any other kind. Finally, the imperfection which takes the form of an initial waviness of the fiber bundle is incorporated by assuming an initial sinusoidal variation in the fiber slope  $\theta = \theta_o$ , given by,

$$\theta_o = e \cos\left(\frac{\pi s}{L}\right) \quad (23)$$

where the imperfection has an amplitude 'e' and a wavelength '2L'. This initial waviness exists without stress and so the shear stress is related to  $\theta - \theta_o$ , as is the moment 'M'. Since the  $\theta$  appearing in the load term of equation 15 is a geometric and not constitutive, it remains unchanged. In almost all the compression strength models an estimate of the initial misalignment angle is critical. In the present work, the angles were experimentally obtained for the individual composites and the procedure as explained previously (Table 1). By following Stief, we substitute equations 16-18 into equation 15 to obtain the following,

$$\theta'' + k \sin \theta - \alpha T_f \tanh\left(\frac{\theta - \theta_o}{T_f}\right) = -e \cos x \quad (24)$$

where,

$$x = \frac{\pi s}{L}$$

$$k = \frac{PL^2}{\pi^2 E_f I}$$

$$\alpha = \frac{4a^2 G_L L^2}{\pi^2 E_f I}$$

$$T_f = \frac{\tau_c}{G_L}$$

The quantity 'x' is the dimensionless arc length, 'k' is the normalized load, 'α' can be viewed as the stresses associated with elastically shearing the matrix relative to those associated with bending the fiber and 'T<sub>f</sub>' is roughly the rotation at which the shearing resistance goes plastic.

Applying the boundary conditions of zero moment at x = 0 and zero slope at x = π/2, or,

$$\theta'(0) = 0, \quad \theta\left(\frac{\pi}{2}\right) = 0$$

and applying a shooting method to solve equation 5. Beginning with θ'(0) = 0 a value of θ(0) = 0 was guessed and the differential equation was solved using the Runge-Kutta method to x = π/2. If θ(π/2) was not zero, the guess was adjusted properly and the solution repeated.

In the present case, the experimentally obtained shear response (see Figure 12) for the different composites were fitted to the same general form presented in equation 17. This was done in an attempt to preserve the general structure of the problem for numerical calculations that were to follow. However, since the strains to failure for the individual composites were so different, the numerical solution scheme had to be modified in order to correctly capture this effect. The solution was split into two sections. In the range from zero strain to the strain to failure, the shear response was prescribed by the fit that was developed in the previous section. In the second section where the strain essentially exceeded the strain to failure, the shear stress was taken to be zero. For the G' sizing for

instance, Figure 14 shows the experimental and fit shear stress versus strain response. The fit does captured the data very well and the corresponding values of the constants are,  $G_L = 4180$  MPa and  $T_f = 0.01105$ . Beyond a strain value of 2%, the shear stress is forced to zero in order to depict complete failure of the specimen. In this manner, the The quantity of interest is the maximum tensile strain  $\epsilon_{total}$  in the bending fiber. This is a sum of two terms namely the bending strain  $\epsilon_{bend}$  that is gotten by solving equation 19 and the compressive strain  $\epsilon_{comp}$ . This is given by,

$$\epsilon_{comp} = -\frac{\pi^2}{2} k \frac{a^2}{L^2} \quad (25)$$

The point at which  $\epsilon_{total}$  becomes equal to the tensile failure strain of the fiber, fiber fracture occurs and the corresponding normalized load 'k' is obtained. The strain to failure for the AS-4 G' lot # D1383-5K was 1.56% and it's tensile modulus was 262 GPa (Table1). The strain to failure for the AS-4 Unsized lot # D1317-4C was 1.63% and its tensile modulus was 252 GPa. The load, P on the fiber was then calculated based on the definition of 'k' in equation 19. Finally, the compression strength of the composite was calculated using the following equation,

$$\sigma_c = \left( E_f v_f + E_m (1 - v_f) \right) \frac{\sigma_f}{E_f} \quad (26)$$

where  $E_f$ ,  $E_m$ ,  $\sigma_f$  and  $v_f$  are the fiber modulus, matrix modulus, stress in the fiber and fiber volume fraction respectively. The matrix modulus was taken to be 3.4 GPa and the fiber volume fraction as measured theoretically was taken to be 0.656 for the G' sizing and 0.61 for both the phenoxy and PVP K90 sizings. Equation 21 further reduces to the following form,

$$\sigma_c = \frac{E_c}{E_f} \frac{P}{\pi a^2} \quad (27)$$

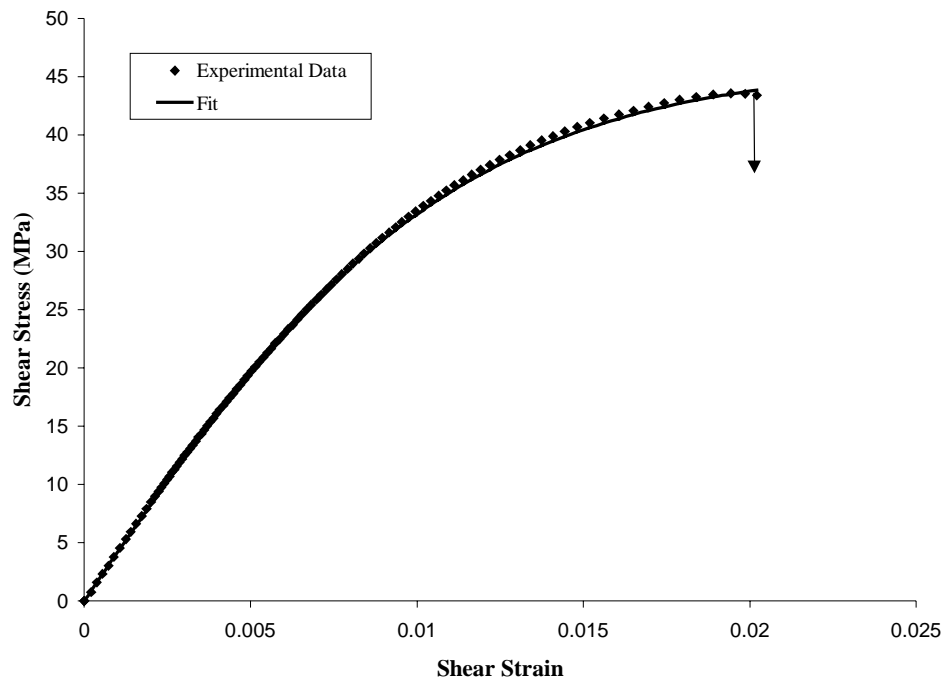


**Figure 14:** Comparison between experimental shear data and recommended tangent hyperbolic fit for the  $G''$  sized composite. The terminal point marks the final stress level at which the code uses the shear stress and strain value from the fit. Beyond this point the shear stress is forced to go to zero indicating failure. The constants for the fit are  $G_L = 4180$  MPa and  $T_f = 0.01105$ .

where,  $E_c$  is the stiffness of the composite. In the absence of an accurate estimate of misalignment length, Table 3 shares the compression strength results from the model for a range of  $L/a$  ratios ranging from 10 to 22 and compares it to that obtained experimentally. The three different composite shear responses were effectively accounted for in the Fortran code that was used to perform the numerical solution.

**Table 3:** Comparison of theoretical (Model 3) and experimental compression strengths at different  $L/a$  ratios for the different unidirectional composites

| Composite Type | $X_c$<br>(in MPa) at<br>$L/a = 10$ | 12                 | 14                 | 16                 | 18                | 22                | $X_c$<br>(in MPa)<br>[Exp.] |
|----------------|------------------------------------|--------------------|--------------------|--------------------|-------------------|-------------------|-----------------------------|
| G'             | 1440.7*<br>(1440.7)**              | 1116.3<br>(1186.1) | 888.5<br>(1008.2)  | 732.6<br>(876.5)   | 609.9<br>(806.2)  | 442.8<br>(705.8)  | 747±110                     |
| PVP K90        | 2501.9<br>(2566)                   | 1782<br>(1871.1)   | 1358.3<br>(1456.2) | 1052.5<br>(1177.8) | 851.4<br>(990)    | 583.2<br>(821.8)  | 934±84                      |
| Phenoxy        | 2561.6<br>(2980.6)                 | 1793.4<br>(2255.9) | 1340.5<br>(1811.2) | 1037.9<br>(1556.7) | 829.3<br>(1416.1) | 567.5<br>(1107.1) | 913±98                      |

\* Stress at which fiber fracture occurs (total strain = tensile strain to failure). This usually occurs after the peak load.

\*\* Peak Stress calculated by reading the peak load

It is also apparent that in addition to the geometric effects example initial misalignment, the composite shear response also plays a role in the determining the compressive properties. The load corresponding to fiber fracture was seen to always occur just after the peak load had been attained, i.e. during the transient kinking stage. Budiansky<sup>8,31</sup> however makes it clear that the compressive strength is not influenced by fiber fracture indicating that the peak load is more important. Thus, from a design standpoint, the peak load is a safer choice. Table 3 therefore also lists the peak compressive stress values in brackets just below the corresponding strength values at fiber fracture. Figure 15 shows a comparative plot of the compressive loading curve for the G', Phenoxy and PVP K90 sized composites. In order to make this comparison an arbitrary value for misalignment angle and  $L/a$  ratio was fixed at 3° and 18 respectively. To check the influence of initial

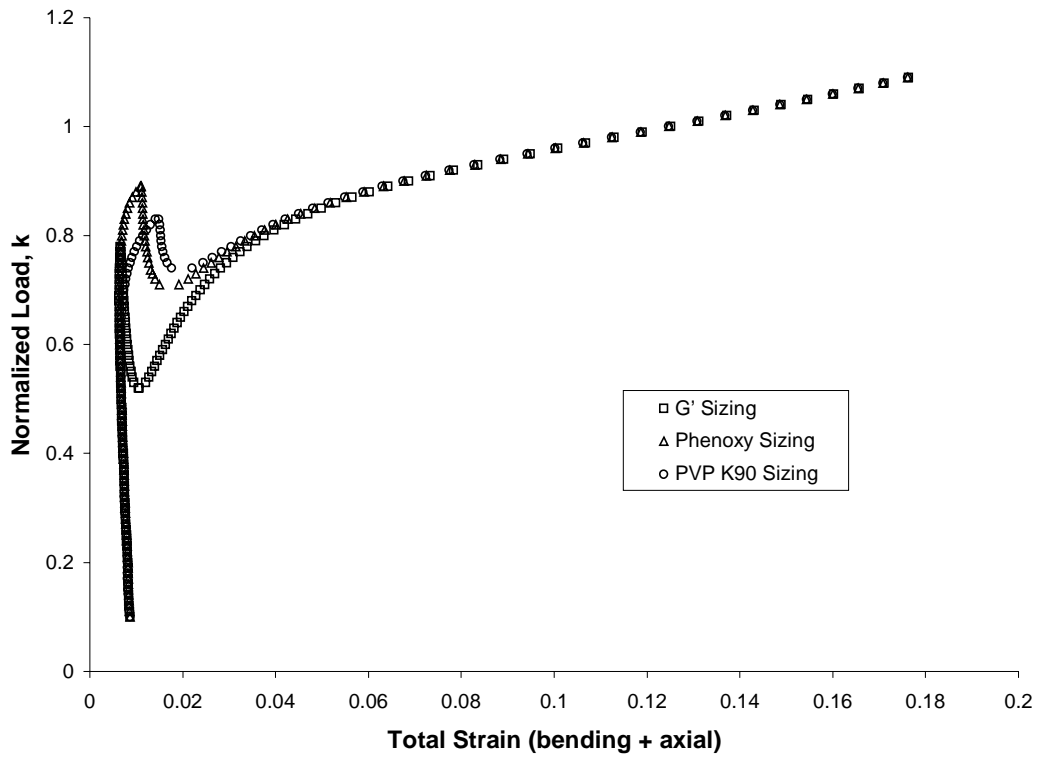


**Figure 15:** The effect of changes in composite shear response on compression loading response according to Model 3 for the three different sizings. A fixed L/a ratio of 18 and initial misalignment angle of  $3^\circ$  was chosen for the simulations

misalignment angle on compression strength, a parametric study was performed on the Phenoxy sized composite. In this study, the L/a ratio was held constant at 18 and misalignment angle of 1.15° (the measured value for the Phenoxy composite), 3° and 5° were input into the code. Figure 16 compares the axial load versus total strain (bending + axial) response as a function of the three misalignment angles for the Phenoxy composite. It is interesting to note that at low misalignment angle the strain does become negative which indicates that the compressive contribution to the strain has a greater influence than the bending portion. This seems only logical as at low angles the fiber is almost straight and cannot participate much in the overall bending process. As the misalignment angle increases however, the strains become completely positive indicating that the bending contribution has taken over. The drop in load beyond the peak load also decreases with increasing misalignment. This is consistent with the observations of Moran et.al<sup>8.32</sup> who claim that while incipient kinking and peak load are extremely sensitive to misalignment and other forms of defects, the steady state kinking stress is relatively insensitive.

### **Tensile properties of the cured blends**

The static tensile properties of the cured K-90 PVP in Derakane™ blends was determined (Figure 17). The static tensile strength was a strong function of the amount of K-90 PVP present in the blend. The initial increase in strength was as great as 30% (55 MPa for pure Derakane™ compared to 71 MPa for 0.25wt% K-90 PVP). The increase in strength at higher K-90 PVP amounts was less dramatic increasing only 5% over the 0.25 to 5.00 wt% K-90 PVP concentrations. Strain-to-failure also showed the same trend. The initial increase was the highest (1.9% strain for pure Derakane™ and 2.75% strain for 0.25wt% K-90) and peaked at a value of 3.2% strain for 5.0wt% K-90 PVP. The tensile modulus was found to be essentially constant over the range of K-90 PVP amounts tested (maximum variation was 7%: 3.44 GPa for the pure Derakane™ and 3.21 GPa for the 0.25 wt% K-90 PVP). From this limited set of data, it can be concluded that even small additions of K-90 PVP to the Derakane™ significantly increases static tensile strength and strain-to-failure without significantly affecting the modulus. This would mean that the toughness of the system denoted by the area under the stress versus strain curve also increases. Utilizing the Cox theory<sup>8.33</sup> this would imply that the combined effect of shear

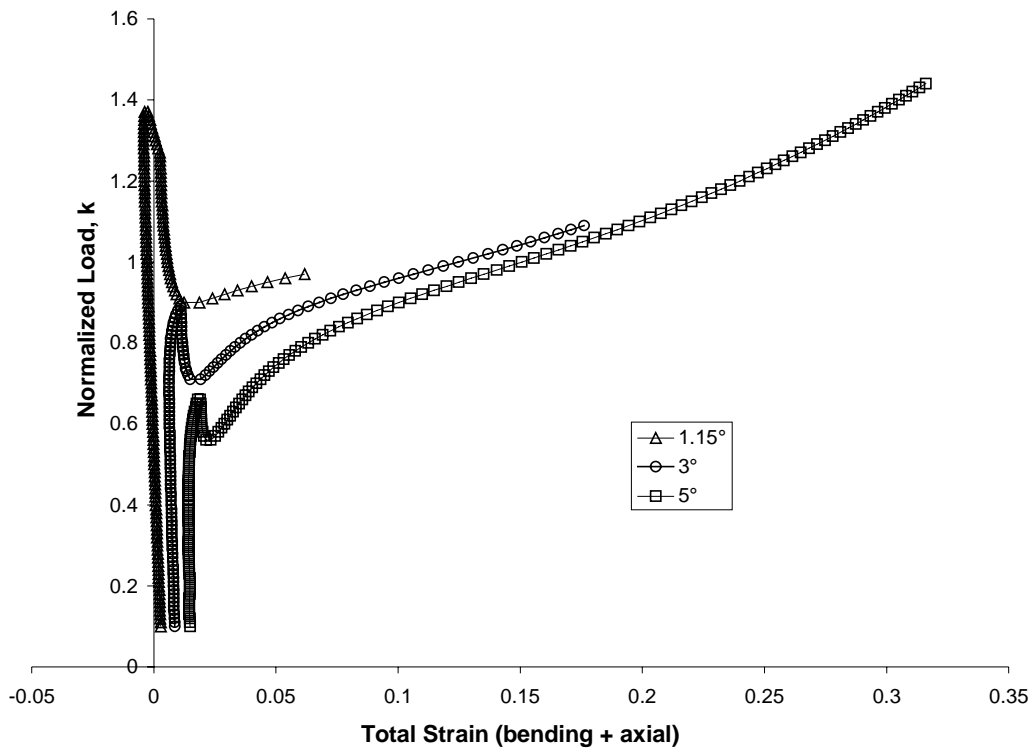
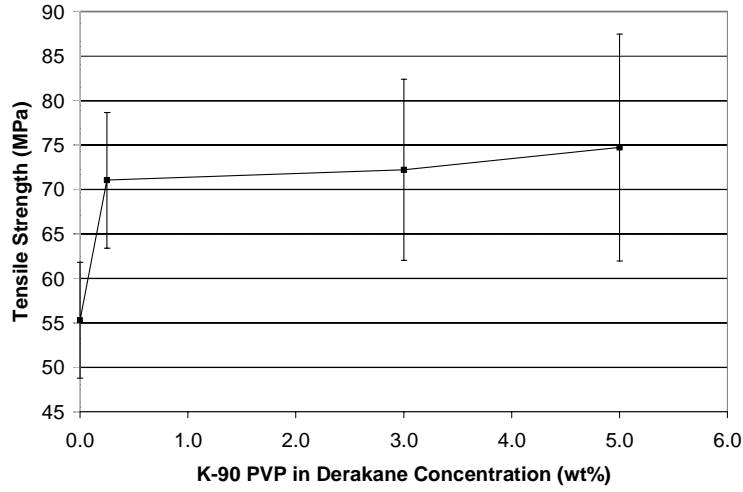
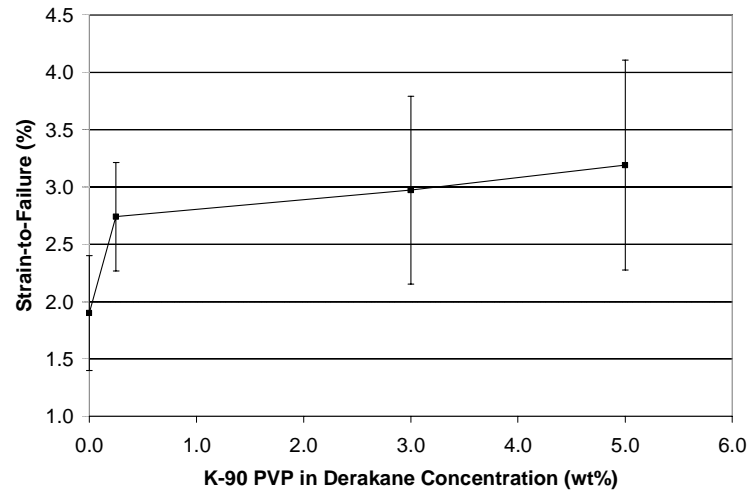


**Figure 16:** The effect of initial misalignment angle on compression loading response according to Model 3 for the Phenoxy composite at an L/a ratio of 18.

a).



b).



c).

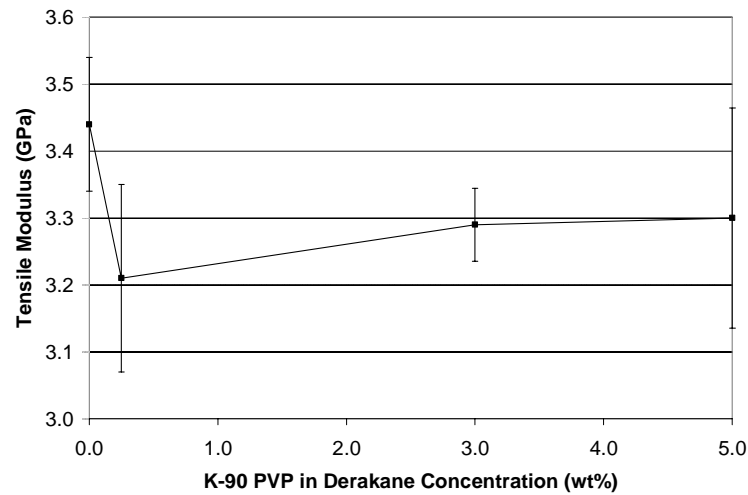


**Figure 17:** Static tensile properties of K-90 PVP in Derakane™ blends. a). Strength b). Strain-to-failure c). Tensile Modulus.

stiffness along with enhanced material toughness of the interphase region of the composite leads to the improvement in axial properties.

## CONCLUSIONS

The addition of small amounts of K-90 PVP to the pure Derakane™ matrix had profound effects on the matrix shrinkage, tensile strength, and tensile strain-to-failure. The matrix shrinkage was found to be a strong function of K-90 PVP concentration. There was a four fold decrease in shrinkage from pure Derakane™ to 5.0wt% K-90 PVP in Derakane™.

The tensile strength was found to increase approximately 30% between the pure Derakane™ and the 0.25wt% K-90 PVP in Derakane without significantly affecting the modulus. The strain-to-failure was found to increase approximately 45% between the pure Derakane™ and the 0.25wt% K-90 PVP in Derakane™. If the Cox theory were applicable, this would imply a drastic improvement in the interfacial shear strength of the composite 'IF' an interphase exists and the Derakane™ constituents do not preferentially separate. This would provide some justification for the improvements in the on-axis properties discussed.

The use of micro-mechanical models to predict both tensile and compressive strength was demonstrated. Although the models did not look at the specifics of the chemical and mechanical composition of the interphase region, they still were able to capture its effects through experimentally obtainable quantities such as the interfacial shear strength, misalignment angle and shear stress-strain response for the different composite systems.

A micro-mechanics based tensile strength model developed by Subramanian, Stinchcomb and Reifsnider was used to predict the strength of the Phenoxy sized composite. Good agreement between experiment and prediction was found to exist (17% error). The influence of the type of sizing was also seen in the  $[\pm 45]_{6s}$  laminate shear data wherein large differences were seen to exist in the shape and magnitude. These differences seemed to influence the compression strength models but not to the same extent as fiber misalignment. Model # 1 formulated by Budiansky was found to predict the compression strength of the PVP K90 composite to within 9% error. The error on the Phenoxy and G" sized composites was a little higher (~15%). This was consistent with the model

assumptions as the PVP system best represented the elastic-perfectly plastic case for which the model had been formulated. Budiansky and Fleck's model, Model#2, although a modification of Model#1, predicted almost the same compression strengths. A model developed by Stief was also used and compression strength predictions made for a range of  $L/a$  ratios in the absence of misalignment length or amplitude measurements at the present time. The implications of fiber misalignment angle on compression strength were found to be profound. The G' sized fiber was measured to have a larger misalignment angle as compared to the Phenoxy and PVP K90 sized fibers. Since the misalignment in the present case was introduced during pultrusion, the importance of handling and protecting the fibers during manufacturing is therefore critical in addition to which the type of sizing can also make a difference.

Changes in composite tension and compression properties are therefore speculated to be influenced by both processing control and interphase. A closer inspection of the gradient nature of the interphase will perhaps increase the accuracy of the predictions.